Organic & Biomolecular Chemistry

Cite this: *Org. Biomol. Chem.*, 2011, **9**, 5394

www.rsc.org/obc

**PAPER**

# The effect of leaving group on mechanistic preference in phosphate monoester hydrolysis†

**Shina C. L. Kamerlin[a] and John Wilkie*[b]**

***Received 20th December 2010, Accepted 21st April 2011***
**DOI: 10.1039/c0ob01210f**

We present 2-dimensional potential energy surfaces and optimised transition states (TS) for water attack on a series of substituted phosphate monoester monoanions at the DFT level of theory, comparing a standard 6-31++g(d,p) basis set with a larger triple-zeta (augmented cc-pVTZ) basis set. Small fluorinated model compounds are used to simulate increasing leaving group stability without adding further geometrical complexity to the system. We demonstrate that whilst changing the leaving group causes little qualitative change in the potential energy surfaces (with the exception of the system with the most electron withdrawing leaving group, $CF_3O^-$, in which the associative pathway changes from a stepwise $A_N + D_N$ pathway to a concerted $A_ND_N$ pathway), there is a quantitative change in relative gas-phase and solution barriers for the two competing pathways. In line with previous studies, in the case of $OCH_3$, the barriers for the associative and dissociative pathways are similar in solution, and the two pathways are equally viable and indistinguishable in solution. However, significantly increasing the stability of the leaving group (decreasing proton affinity, PA) results in the progressive favouring of a stepwise dissociative, $D_N + A_N$, mechanism over associative mechanisms.

## Introduction

Phosphate ester hydrolysis is a crucially important process for several biological systems, as it is involved in energy and signal transduction processes, the control of cellular metabolism, and the regulation of protein function.[1–3] In its simplest form, phosphate monoester hydrolysis involves the symmetric displacement of an oxygen-based ligand by hydroxide or water (Scheme 1). Scheme 1 is deceptively simple, however, and the characterisation of all possible ways in which phosphate monoester cleavage can occur is far from trivial.

$$HO^- + RPO_4^{2-} \rightleftharpoons [RHPO_5]^{3-} \rightleftharpoons HPO_4^{2-} + OR^-$$

**Scheme 1** Model reaction for phosphate ester hydrolysis.

Conventionally, this reaction can be generalised into two different pathways (Scheme 2). In the dissociative pathway (A, Scheme 2), leaving group departure precedes nucleophilic attack, and the reaction proceeds *via* a metaphosphate intermediate. Formally, this may be termed a $D_N + A_N$ mechanism. Alternately, the phosphorous atom may use its empty low lying d-orbitals to engage in p–d bonding, allowing for pentavalent phosphorous species as intermediates in the hydrolysis mechanism. This leads to a potential associative pathway in which nucleophilic attack occurs prior to the departure of the leaving group, formally termed an $A_N + D_N$ mechanism. Both these pathways, however, are stepwise processes, and the reaction can also proceed *via* concerted pathways (*i.e.*, $A_ND_N$ mechanisms), which proceed through a single transition state with partial bond formation to the nucleophile and partial bond breaking to the leaving group, and no transition state. The $A_ND_N$ pathways can, in turn, be either associative or dissociative in nature, and their classification as such is dependent on the topology of the relevant free energy surface, that is, whether bond formation or bond cleavage dominates as the transition state is approached. Here, it is important to clarify a slight complication that arises from the non-linear relationship between bond order and bond length.[4] That is, a process that is described as "associative" in terms of bond length (*i.e.*, the physical separation of $O_{nuc}$ from $O_{lg}$ at TS is less than at either reactant or product states) may also be identified as "dissociative" in terms

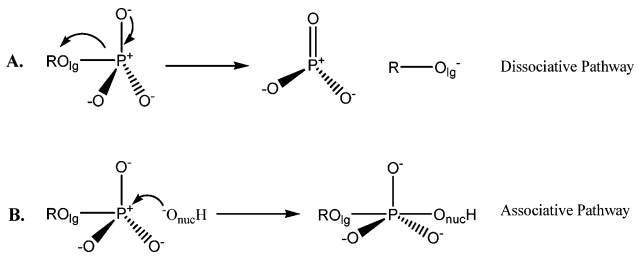


**Scheme 2** Reaction pathways for phosphate monoester hydrolysis.

[a]*Department of Organic Chemistry, Arrhenius Laboratory, Stockholm University, S-10691 Stockholm, Sweden*
[b]*School of Chemistry, University of Birmingham, Edgbaston, Birmingham, B15 2TT, UK. E-mail: j.wilkie@bham.ac.uk; Fax: +44 (0)121 414 4403; Tel: +44 (0)121 414 7189*

† Electronic supplementary information (ESI) available. See DOI: 10.1039/c0ob01210f

of bond order, if the combined bond orders for P–$O_{nuc}$ and P–$O_{lg}$ are less than 1 (an example of how shifting between a bond distance and bond order representation changes the topology of the free energy surface is shown in ref. 5). Thus, in the case of the concerted pathways, experimental observations, such as $\beta_{lg}$, that are largely dependent on bond order, may indicate a "dissociative" pathway for a process that is clearly associative in terms of bond distances. In this work, we have focused on bond length rather than bond order, as our ultimate interest lies in understanding enzyme catalysis, where geometry can play a significant role. Note also, however, that as there is a potential continuum of TS of varying degrees of "associative" and "dissociative" character in the case of a concerted process, the use of these terms has resulted in significant confusion amongst readers and in the interpretation of the experimental data. Therefore, it should be pointed out that when describing the nature of a transition state as being "associative" or "dissociative", it is insufficient to take simply the structure of the isolated transition state into account, but rather, it is necessary to examine the topology of the relevant free energy surface and to also examine the pathway by which this transition state was reached. This was again illustrated in, *e.g.*, ref. 5 (amongst other works), and is the approach we have followed here.

Finally, the reaction can either proceed *via* an inline or a non-inline pathway, leading to a total of eight distinct reaction mechanisms. However, since earlier work has demonstrated that the barriers for both inline and non-inline processes are fairly similar,[6] only the inline pathways have been considered in this work, as was also the case in our previous study[7]

In recent years, many phosphatases have become identified as key drug targets for a range of diseases including but not limited to diabetes, obesity, neurodegenerative diseases, as well as for cancer therapy,[8,9] and have thus become the focus of intensive research. Similarly, much effort has also been employed towards the design of artificial catalysts for phosphate ester hydrolysis (which are often modelled on known enzyme structures).[10–12] Clearly, understanding factors that affect the mechanism of phosphate hydrolysis and the selectivity of related enzymes is of key importance. However, despite decades of research into this field, the precise mechanisms of even non-enzymatic phosphate ester hydrolysis remain unclear, partially due to the fact that the relatively high energies of the transition states involved in phosphate hydrolysis make the characterisation of such transition states experimentally very difficult. Also, even for extensively studied systems, there is a lot of controversy surrounding the preferred mechanism. For instance, experimental studies have long claimed that the hydrolysis of monoesters in aqueous solution follows a largely dissociative mechanism, on the basis of a large negative value of $\beta_{lg}$,[13,14] as well as a near zero-entropy of activation.[15] However, the value of activation entropies in distinguishing between associative and dissociative pathways has been questioned,[16] and it has been demonstrated that associative and dissociative transition states for the hydrolysis of phosphate monoester dianions have similar activation entropies.[17] Also, theoretical studies on model systems have proposed both $D_N + A_N$[18] and $A_N + D_N$[19–21] mechanisms for monoester hydrolysis in solution. More explicitly, the only studies that simultaneously consider both associative and dissociative pathways for the hydrolysis of phosphate esters in solution with a variety of leaving groups have shown that the mechanism is largely dependent on the acidity of the leaving group, preferring a more associative mechanism at higher p$K_a$ and switching to a dissociative mechanism as the p$K_a$ of the system decreases,[22,23] despite accurately reproducing experimental LFER, strengthening previous propositions that Brønsted linear free energy relationships do not have unique mechanistic interpretations.[16,24,25]

Computational studies on the hydrolysis of phosphate esters in aqueous solution have suggested that the associative and dissociative pathways have similar barriers.[17,22,24] Here, we extend on these previous studies, and present 2-dimensional potential energy surfaces for water attack on a series of substituted phosphate monoester monoanions, with progressively more electron withdrawing leaving groups. By mapping the full potential energy surface, we are able to directly compare the associative pathways to the dissociative pathways in the presence of a nucleophile.

The potential energy surfaces were used to identify the approximate location of key stationary points which were then optimised in the gas phase in the absence of constraints. Solvation effects were subsequently simulated by means of performing a solvation correction to the SCF energy using a continuum model rather than by including explicit water molecules, in order to avoid the introduction of additional degrees of freedom into the system. This approach was previously successfully applied to studying the effect of metal ions on water exchange on the phosphate monoanion[5] and a similar approach was applied to related studies of phosphate hydrolysis.[7,17,22,23,26]

## Methodology

### Reacting systems

In our previous work,[7] we examined water exchange on the phosphate monoanion ($H_2PO_4^-$). Here, we are extending our previous study to include water attack on phosphate monoanions with a variety of different leaving groups, as outlined in Scheme 3. We have ranked our systems by the proton affinity (PA) of the leaving group. Whilst proton affinities are very difficult to determine experimentally, obtaining reliable values for the proton affinity by computational approaches is fortunately facile,[27] albeit highly dependent on the level of theory used. Simply, the PA for each of the systems shown in Scheme 3 can be calculated using eqn (1):

$$PA = -\Delta H = -\Delta E + RT \quad (1)$$

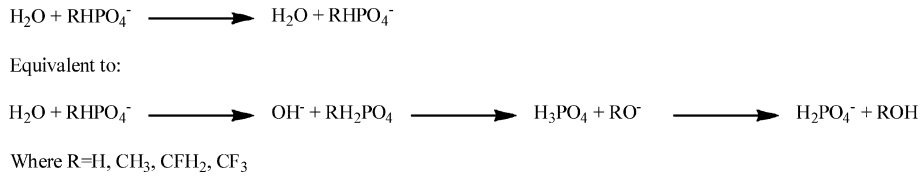


**Scheme 3** Model systems for phosphate monoester hydrolysis.

Here, $\Delta E$ represents the internal energy of a non-linear polyatomic molecule, which can be approximated from eqn (2):

$$E_{tot} = E_{rot} + E_{trans} + ZPE + E'_{vib} + E_{elec} \quad (2)$$

ZPE represents the zero point vibrational energy, which can be obtained by calculating the gas phase vibrational frequencies. The contributions from $E_{rot}$ and $E_{trans}$ (rotational and translational energies) to the total energy both equal $3/2RT$ (from statistical mechanics). The change in electronic affinity can therefore be obtained from eqn (3):

$$\Delta E_{elec} = E_{elec}(ROH) - E_{elec}(RO^-) \quad (3)$$

Finally, the contribution from $E'_{vib}$ (vibrational energy) is negligible when compared to the ZPE, and the proton does not possess rotational kinetic energy, keeping $E_{rot}$ constant. Therefore, the proton affinity is calculated from eqn (4):

$$PA = -\Delta E_{elec} - \Delta ZPE + 5/2RT \quad (4)$$

The potential energy surface (PES) for phosphate monoester hydrolysis in each of our systems is represented on a More O'Ferrall–Jencks plot, MFJ,[28,29] as shown in Fig. 1. Here, the energy surface is defined in the terms of two reaction coordinates, namely the distance between the phosphorous atom and the leaving group (P–$O_{lg}$, *x*-axis) and nucleophile (P–$O_{nuc}$, *y*-axis) oxygen atoms, respectively. This allows us to directly compare the different mechanistic possibilities (*i.e.*, associative *vs.* dissociative, stepwise *vs.* concerted) on the same PES, whilst simultaneously providing information about the relative energetics of the different pathways. The resulting PES was then used to identify the key stationary points for each system, which were then optimised without constraints and used to obtain precise reaction barriers.

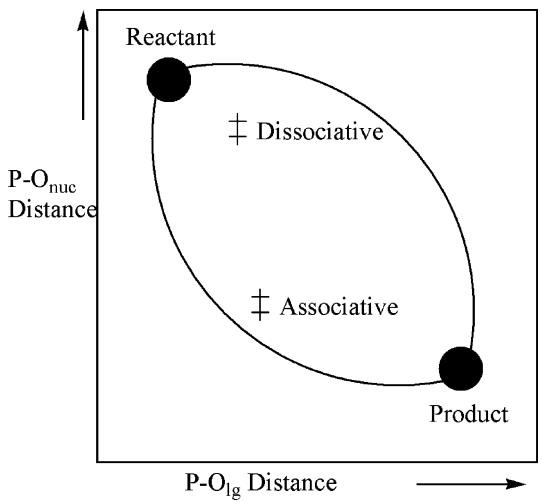


**Fig. 1** Schematic potential energy surface, showing positions of reactant and product, along with indications of typical associative and dissociative pathways.

### Computational approaches

All *ab initio* calculations in this work have been performed using the Gaussian03 (G03) software package,[30] either a conventional 6-31++G(d,p) basis set[31] or Dunning's correlation consistent, triple zeta basis set cc-pVTZ augmented with diffuse functions[32] and a combination of Barone's 1-parameter modified Perdew–Wang 91 exchange functional[33] and the Perdew–Wang 91 correlation functional (MPW1PW91).[34] It should be noted that we chose this functional rather than the more common and popular B3LYP[35,36] functional as, in a prelude[37] to our previous work,[7] a comparative study of different functionals and basis sets suggested that this combination provides the most stable and reliable results (while avoiding problems with unbound electrons, which we observed for, for instance, B3LYP). By comparison, the MPW1PW91 functional gave no such problems. At each point on the More O'Ferrall–Jencks plot, the two distances defining the reaction coordinate were frozen while all other degrees of freedom where allowed to freely optimise. Since the More O'Ferrall–Jencks plot is a projection of the full PES onto 2 dimensions, any one point on the More O'Ferrall–Jencks plot can correspond to multiple points on the full PES and any variation in the extra degrees of freedom not directly involved in bond making or breaking can add noise to the More O'Ferral–Jencks plot, obscuring the location of key features on the PES. In order to avoid this problem, we generated our More O'Ferrall–Jencks plots by careful reaction coordinate pushing and at each point, the geometry and energy of the resulting structure was examined in order to verify that it is the true minimum energy structure for that point on the 2-dimensional plot (see also, *e.g.*, ref. 5, 7, 17, 22, 23, 26). By selecting the methoxy group as our leaving group, we were able to keep any additional degrees of freedom to a minimum. Furthermore, by progressively replacing H-atoms with more electronegative F-atoms, we were able to modify the proton affinity of our ligand while neither changing the complexity of our leaving group, nor significantly altering its bulk.

Approximate geometries of key stationary points were obtained from the nearest constrained optimised structure on the PES, and these structures were then subjected to a fully unconstrained optimisation. Obtaining unconstrained dissociative transition states is particularly challenging as the PES becomes quite flat with increasing P–O distance. Therefore, these transition states were optimised using the GDIIS algorithm of Csaszar and Pulay.[38] Finally, solvation effects were simulated by applying a PCM correction to key stationary points following the method of Tomasi (for a review see ref. 39 and references cited therein) and re-optimising. We have used the UFF model, as this model defines hydrogen atoms explicitly[40] and a number of the obtained transition states also included some degree of proton transfer. Setting the solvent to "water" results in a dielectric of 78.3553. Transition states and local minima were characterised by means of the calculation of vibrational frequencies on the fully optimised (unconstrained) stationary points in both solution and gas phase with all transition states showing exactly one negative eigenvalue and minima none. Transition states were further characterised by following the intrinsic reaction coordinate in both directions and minimising to reveal appropriate reactant, product or intermediate complexes. In the case of gas phase calculations, IRCs all terminated in reactant, product and intermediate structures corresponding to those determined from the initial PES. For PCM optimised transition states, this situation is a little different: in all cases, IRCs from PCM optimised transition states give reactant or product complexes that correspond to those seen in the initial PES as do associative intermediates, but in determining dissociative mechanisms, we find that the potential energy surface has changed at long P–$O_{nuc}$ and P–$O_{lg}$ distances, resulting in

 

**Table 1** Leaving groups ranked in order of decreasing proton affinity determined at 298 K. ΔPA is the proton affinity of each leaving group relative to hydroxide. All values are given in kcal mol$^{-1}$

| Leaving group | Proton affinity (PA) | ΔPA |
|---|---|---|
| $^{-}$**OH** | 393.1 | 0.00 |
| $^{-}$**OCH$_3$** | 382.0 | −10.8 |
| $^{-}$**OCFH$_2$** | 365.9 | −27.2 |
| $^{-}$**OCF$_3$** | 325.6 | −67.5 |

dissociative intermediates that differ from those observed in the gas phase PES. It is these IRC-derived intermediates that are shown in the relevant figures and discussed in the text.

Gas phase vibrational frequency calculations were also used to obtain zero-point vibrational energies which are necessary for the calculation of the proton affinity of each leaving group.

Basis set superposition errors have been calculated for an example reaction using the counterpoise keyword.

## Results and discussion

### Ranking of the reacting systems

The stability of the developing negative charge can be assessed from the proton affinity (PA) of the leaving group anion, which is defined as the negative of the enthalpy change under standard conditions (*i.e.*, 298 K and 1atm). Table 1 shows the leaving groups for the systems examined in this work, ranked in order of decreasing proton affinity. This trend follows the fact that the electronegativity of the leaving group systematically increases upon descending the table, due to the presence of the highly electronegative fluorine atoms. Decreasing the proton affinity of the leaving group increases the leaving group ability (as the leaving group becomes more electron withdrawing), therefore, intuitively one would expect an increased preference for a dissociative reaction pathway upon descending Table 1.

### Phosphate ester hydrolysis, RHPO$_4^-$, R = H

The PES for water attack on $H_2PO_4^-$ (Fig. 2) was discussed extensively in our previous study,[7] and, in common with that work, the energies discussed in detail here are those from 6-31++g(d,p) optimisations. Where the two works differ is in the treatment of solvation—here we have allowed the structures of the stationary points to optimise within the PCM model, and so "solution phase" and gas phase structures may differ. The reaction was found to proceed *via* either a stepwise associative ($A_N$ + $D_N$) mechanism with a barrier of 38.5 kcal mol$^{-1}$ in the gas phase or 35.8 kcal mol$^{-1}$ in solution (a negligible reduction of 0.3 kcal mol$^{-1}$ compared with the single point model in ref. 7), or a stepwise dissociative ($D_N$ + $A_N$) mechanism. From the PES (Fig. 2), an approximate transition state can be observed at P–$O_{lg}$ ~ 2.2 Å and P–$O_{nuc}$ ~ 3.2 Å. However, in our previous study, we were unable to obtain unconstrained dissociative transition states due to SCF convergence issues at long P–O distances. Here, using direct inversion in the iterative subspace (GDIIS), we were able to identify an unconstrained gas phase transition state with P–O distances of 1.99 and 3.16 Å to the leaving group and nucleophile, respectively. Upon optimisation in the continuum model, the corresponding bond lengths changed to 1.82 and 3.15 Å (Fig. 3).

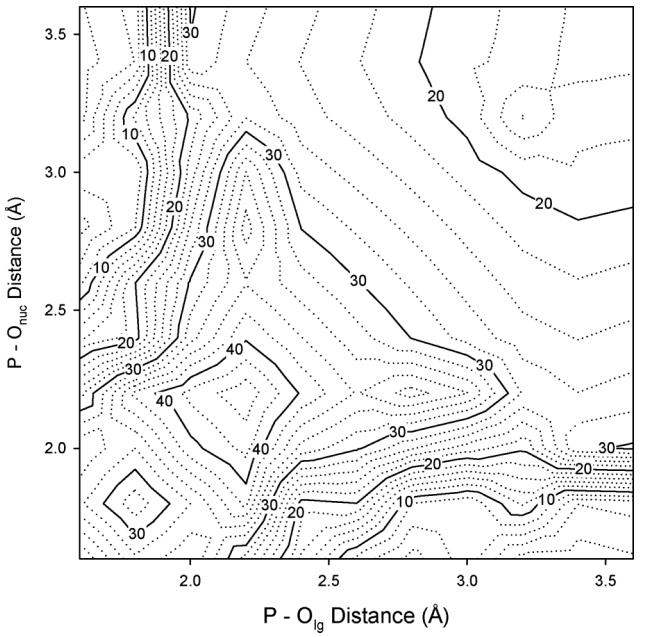


**Fig. 2** PES for water attack on RHPO$_4^-$ where R = H. The reactant structure lies towards the upper left corner and the product towards the lower right.

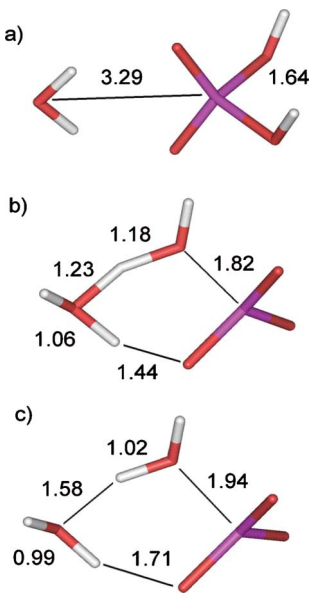


**Fig. 3** Stationary points for $H_2O$ attack on RHPO$_4^-$, where R = H, $D_N$ + $A_N$ pathway. Shown are: (a) the reactant complex; (b) the dissociative TS and (c) the asymmetric intermediate.

This is as would be expected, in light of the fact that the continuum model is now shielding some of the charge on the departing oxyanion. The transition state optimized in the continuum model is lower in energy than both the single point PCM-corrected and PCM-optimised structures of the gas phase intermediate so it is clear that there has been some modification to the PES at long P–O distances. Following the IRC from the PCM-optimised transition state and optimising to local minima revealed an alternative, asymmetric dissociative intermediate with P–O distances of 1.94 and 3.38 Å, lying ~1.7 kcal mol$^{-1}$ below the dissociative transition

**Table 2** Energies and key geometric parameters of stationary points for water attack on $RHPO_4^-$ where R = H. Here, RC denotes a reactant complex, TS denotes a transition state, Int. denotes an intermediate, Asym. Int. denotes the asymmetric intermediate found from the IRC with PCM. Parenthesised values indicate PCM optimised results

| | Associative pathway | | | Dissociative pathway | | | |
|---|---|---|---|---|---|---|---|
| | RC | $A_N + D_N$TS | $A_N + D_N$ Int. | RC | $D_N + A_N$ TS | $D_N + A_N$ Int. | $D_N + A_N$ Asym. Int. |
| **P–$O_{nuc}$/Å** | 3.33 (3.29) | 2.18 (2.23) | 1.77 (1.76) | 3.33 (3.29) | 3.16 (3.15) | 3.42 | (3.38) |
| **P–$O_{lg}$/Å** | 1.66 (1.64) | 1.71 (1.67) | 1.77 (1.76) | 1.66 (1.64) | 1.99 (1.82) | 3.42 | (1.94) |
| **Total energy/Hartree** | −719.99701 | −719.93574 | −719.95491 | −719.99701 | −719.95408 | −719.97302 | (−720.07217) |
| **ΔH/kcal mol$^{-1}$** | 0 | 38.5 | 26.4 | 0 | 26.9 | 15.1 | — |
| **ΔH (PCM)/kcal mol$^{-1}$** | 0 | 35.8 | 25.7 | 0 | 19.8 | — | 18.1 |

state. As the overall reaction in this case is symmetrical, there should be a further, mirror image, intermediate in which the lengths of the making and breaking bonds are reversed, and these two intermediates should be connected by an additional transition state, rendering the dissociative pathway a three-step pathway (bond breaking—reorganisation—bond making). Unfortunately, as this additional transition state involves no bond making or breaking events, but rather the reorganisation of weakly bound fragments, it is extremely difficult to determine its structure. However, as it does not involve bond making or breaking events we do not anticipate that its energy differs greatly from that of the asymmetrical intermediate and that it will be of lower energy than the bond making or bond breaking transition states already identified. Table 2 shows a summary of the key geometric parameters and energies of the stationary points for both the associative and dissociative reaction pathways both in the gas phase and in solution. Thus, it would appear that the dissociative pathway is preferred by 16.0 kcal mol$^{-1}$ in solution. Reoptimisation of all stationary points with the considerably larger augmented cc-pVTZ basis set resulted in no discernible change in gas phase geometries or energies (the change in the barrier height is again negligible, increasing by 0.3 kcal mol$^{-1}$ for the associative pathway, and 0.6 kcal mol$^{-1}$ for the dissociative pathway). The situation is similar in the continuum model, where once again we see no discernible change in stationary point geometries, and only a slight change in energy, with barrier heights increasing by 0.4 and 1.5 kcal mol$^{-1}$, respectively.

### Phosphate ester hydrolysis, $RHPO_4^-$, R = $CH_3$

The PES for water attack on methyl phosphate is shown in Fig. 4. ΔPA (relative to R = H) is −11 kcal mol$^{-1}$ and the PESs for water attack on $H_2PO_4^-$ (Fig. 2) and methyl phosphate (Fig. 4) are qualitatively similar. Once again, the PES is split into two stepwise $A_N + D_N$ and $D_N + A_N$ reaction pathways, with a high energy hill separating the two pathways.

The PCM optimised stationary points for the $A_N + D_N$ pathway are shown in Fig. 5. In the reactant complex (Fig. 5a), P–$O_{lg}$ is 1.64 Å and P–$O_{nuc}$ is 3.30 Å. In addition, the attacking water molecule forms a hydrogen bond to one of the phosphate oxygen atoms. The first associative transition state (Fig. 5b) corresponds to the formation of the P–$O_{nuc}$ bond, and the P–$O_{nuc}$ distance in this transition state is 2.20 Å. However, in our simulations, we observe that P–O bond formation is coupled with proton transfer from the attacking water molecule to the phosphate, *via* the pre-existing hydrogen bond in the reactant complex. The barrier to this transition state is 38.5 kcal mol$^{-1}$ in the gas phase and

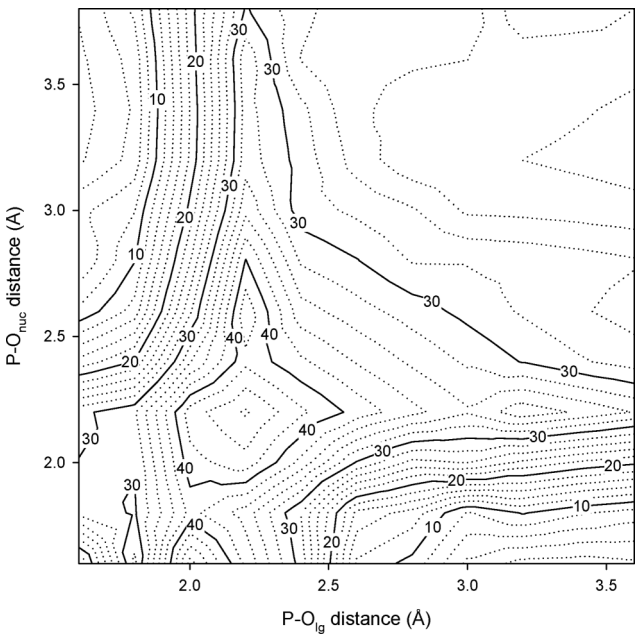


**Fig. 4** PES for water attack on $RHPO_4^-$ where R = $CH_3$. Reactant complex lies towards the upper left corner, product towards the lower right.

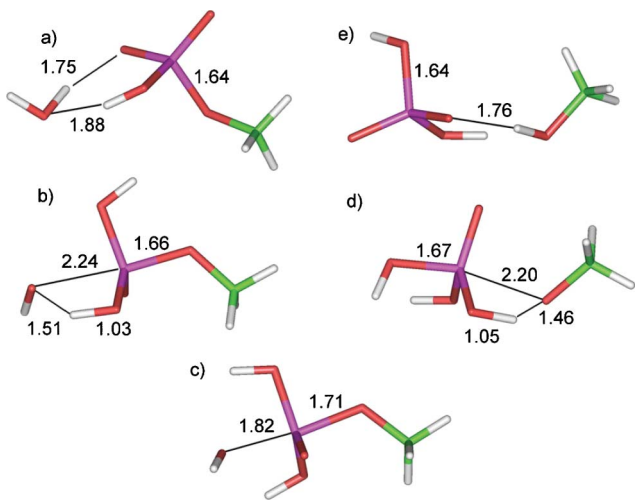


**Fig. 5** Stationary points for $H_2O$ attack on $RHPO_4^-$, where R = $CH_3$, $A_N + D_N$ pathway. Shown are: (a) the reactant complex; (b) the TS for P–OH formation; (c) the associative intermediate; (d) the TS for P–$OCH_3$ breaking and (e) the product complex.

 

38.2 kcal mol$^{-1}$ correcting for solvent. In contrast to the previous system, which proceeded through a symmetrical associative intermediate with P–O distances of 1.76 Å to both nucleophile and leaving group, the associative intermediate for water attack on methyl phosphate state (Fig. 5c) is an asymmetric intermediate with P–O distances of 1.82 Å to the nucleophile and 1.71 Å to the leaving group. In the second associative transition state (leaving group departure, Fig. 5d), P–$O_{nuc}$ = 1.67 Å and P–$O_{lg}$ = 2.20 Å), P–$O_{lg}$ cleavage is again coupled with proton transfer, this time from a phosphate oxygen onto the leaving group, yielding $H_2PO_4^-$ and methanol as products (Fig. 5e, P–$O_{nuc}$ = 1.64 Å and P–$O_{lg}$ = 3.29 Å).

The PCM optimised stationary points for the $D_N + A_N$ pathway are shown in Fig. 6. The reactant and product complexes (Fig. 6a and 6f) are the same as those shown for the $A_N + D_N$ pathway (Fig. 5). The first $D_N + A_N$ transition state, corresponding to P–$O_{lg}$ cleavage (Fig. 6b), is very similar for the previous system where R = H (Fig. 3b). In this transition state, P–$O_{lg}$ = 1.80 Å and P–$O_{nuc}$ = 3.13 Å). As was the case for R = H, P–$O_{lg}$ cleavage is associated with proton transfer. One proton is transferred directly from the water molecule to the leaving group, forming methanol, while a second proton is transferred from a phosphate oxygen to the water molecule, both along pre-existing hydrogen bonds. The barrier for P–$O_{lg}$ cleavage is 26.8 kcal mol$^{-1}$ in the gas phase and 21.3 kcal mol$^{-1}$ with a PCM correction. As the water molecule attacks the phosphorous atom in the second step (transition state, Fig. 6e, P–$O_{nuc}$ = 1.86 Å and P–$O_{lg}$ = 3.85 Å), it transfers a proton along this hydrogen bond, once again yielding $H_2PO_4^-$ and methanol as products (Fig. 6f). It is this second step, nucleophilic attack, that turns out to be rate limiting with a corrected barrier of 39.0 kcal mol$^{-1}$.

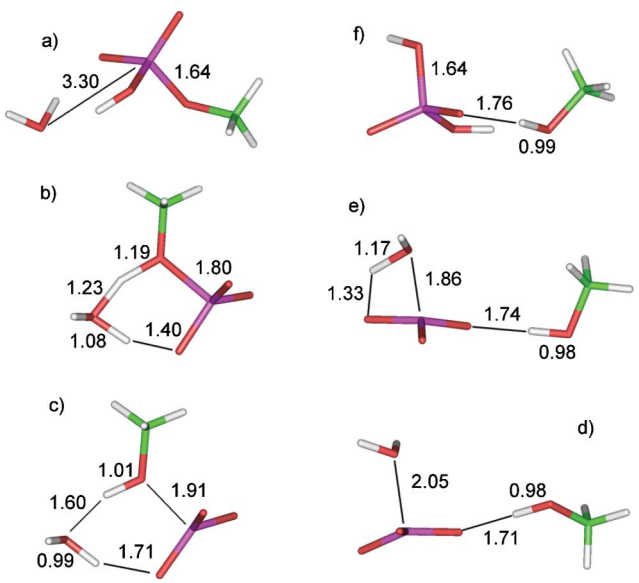


**Fig. 6** Stationary points for $H_2O$ attack on $RHPO_4^-$, where R = $CH_3$, $D_N + A_N$ pathway. Shown are: (a) the reactant complex; (b) the TS for P–$OCH_3$ breaking; (c) the first asymmetric intermediate; (d) the second asymmetric intermediate; (e) the TS for P–OH formation and (f) the product complex.

As with the previous example, R = H, we see a modification of the PES at long P–$O_{nuc}$ and P–$O_{lg}$ on inclusion of a PCM correction. Following the IRC from both transition states, we identify a pair of asymmetric intermediates (Fig. 6c and 6d) with P–$O_{nuc}$ = 3.33 Å, P–$O_{lg}$ = 1.91 Å and P–$O_{nuc}$ = 2.04 Å, P–$O_{lg}$ = 3.85 Å, respectively. As was the case for R = H, both intermediates are close in energy to the transition state for leaving group departure and we proved unable to identify a transition state for the reorganisation linking them. The energies and geometries of key stationary points are summarised in Table 3.

Once again, optimisation with the larger triple zeta basis set produces no discernable change in stationary point geometries though total energies are approximately 0.2 Hartree lower than for the smaller 6-31++g(d,p) basis set, as might be expected. However, this reduction in energy is seen for all structures and so relative energies change to a much smaller degree, with barrier heights for both associative and dissociative processes being increased by only 0.7 kcal mol$^{-1}$.

Florián and Warshel[25] have previously proposed that water attack on methyl phosphate may proceed in a stepwise fashion *via* a substrate-as-base mechanism, in which an initial pre-equilibrium proton transfer from the attacking water molecule to the phosphate generates hydroxide as a nucleophile, which subsequently attacks a neutral phosphate, though this proposition met with some controversy.[41] An earlier study examined whether the proposal of Florián and Warshel[25] also holds in the case of phosphate diesters and demonstrated that such a pathway is viable for dineopentyl phosphate hydrolysis.[4] Here, in line with the findings of Florián and Warshel,[25] we once again show that both the $A_N + D_N$ and $D_N + A_N$ reaction pathways proceed *via* a substrate-as-base mechanism, with proton transfer within the reacting complex.

The barrier heights for the solvated $A_N + D_N$ and $D_N + A_N$ pathways differ by only 0.2 kcal mol$^{-1}$, which is within the limit of reliability of this methodology. This is does not fit with the interpretation of experimental data offered by Westheimer[42] and others which suggests that the reaction proceeds through a dissociative mechanism involving the formation of a monoanionic metaphosphate intermediate ($PO_3^-$). However, it is noticeable that these early works do not consider an associative pathway to be a viable mechanism at all. In contrast, our findings support those of Florián and Warshel,[25] who, using a different computational approach, find an equally small preference but for the $A_N + D_N$ process. As they pointed out,[25] these differences are too small for absolute confidence, and thus both mechanisms are viable, with the final selection between them depending on the specific electrostatic environment. It should also be noted that the analysis of experimental information with regard to phosphoryl transfer reactions is quite complex, and does not have a straightforward interpretation, as discussed in detail in ref. 16. The experimentally determined rate constant for the hydrolysis of methyl phosphate is $8 \times 10^{-6}$ s$^{-1}$ at 373 K and pH 4.2,[43] giving a value of 30.7 kcal mol$^{-1}$ for $\Delta G_{exp}$. This is rather less than our calculated overall barrier of 39.0 kcal mol$^{-1}$ for the $D_N + A_N$ process. Closer inspection of the transition states reveals that the TS for leaving group departure (first step, $D_N + A_N$) has undergone substantial rearrangement with respect to the reactant complex and now resembles a TS for a non-inline displacement with the water molecule effectively catalysing the transfer of a proton from phosphate to leaving group. The second transition state (attack of nucleophile) shows no equivalent catalysis by the now departed leaving group with the

**Table 3** Energies and key geometric parameters of stationary points for water attack on $RHPO_4^-$ where R = $CH_3$. Here, RC denotes a reactant complex, TS denotes a transition state, Int. denotes an intermediate, Asym. Int. denotes the asymmetric intermediate found from the IRC with PCM. Parenthesised values indicate PCM optimised results

| | Associative pathway | | | | | Dissociative pathway | | | | | | |
|---|---|---|---|---|---|---|---|---|---|---|---|---|
| | RC | $A_N + D_N$ TS (1) | $A_N + D_N$ Int. | $A_N + D_N$ TS (2) | PC | RC | $D_N + A_N$ TS (1) | $D_N + A_N$ Asym. Int. 1 | $D_N + A_N$ Int. | $D_N + A_N$ Asym. Int. 2 | $D_N + A_N$ TS (2) | PC |
| **P–$O_{nuc}$/Å** | 3.37 (3.30) | 2.20 (2.24) | 1.91 (1.82) | 1.71 (1.67) | 1.66 (1.64) | 3.37 (3.30) | 3.11 (3.13) | (3.33) | 3.40 | (2.04) | 2.01 (1.86) | 1.66 (1.64) |
| **P–$O_{lg}$/Å** | 1.66 (1.64) | 1.71 (1.66) | 1.70 (1.71) | 2.20 (2.20) | 3.32 (3.29) | 1.66 (1.64) | 1.97 (1.80) | (1.91) | 3.85 | (3.85) | 3.82 (3.85) | 3.22 (3.29) |
| **Total energy/Hartree** | −759.28800 | −759.22658 | −759.24407 | −759.22641 | −759.28853 | −759.28800 | −759.24517 | (−759.36180) | −759.26013 | (−759.35177) | −759.22988 | −759.28853 |
| **ΔH/kcal mol$^{-1}$** | 0 | 38.5 | 27.6 | 38.7 | −0.3 | 0 | 26.8 | — | 17.5 | — | 36.5 | −0.3 |
| **ΔH (PCM)/kcal mol$^{-1}$** | 0 | 38.2 | 29.0 | 39.2 | 0.4 | 0 | 21.3 | 19.1 | — | 25.4 | 39.0 | 0.4 |

proton transferred directly from the water molecule to phosphate. This is a drawback of a system that includes only a single explicit water molecule, primarily acting as the nucleophile, but as discussed in our conclusions, inclusion of a mixed implicit and explicit solvent model leads to its own problems.

### Phosphate ester hydrolysis, $RHPO_4^-$, R = $CFH_2$

When R = $CFH_2$, ΔPA is –27.2 kcal mol$^{-1}$, almost double that for R = $CH_3$. However, as can be seen from Fig. 7, once again, there is little qualitative change in the PES, and the energy surface is split into two stepwise pathways. Both the $A_N + D_N$ and the $D_N + A_N$ pathways involve proton transfer from the nucleophile and to the leaving group, respectively, in precisely the same fashion as was observed when R = $CH_3$. Table 4 shows the energies and geometries of key stationary points, and the structures for the key stationary points are shown in Fig. 8 and 9. There is now a clear preference for the $D_N + A_N$ pathway over $A_N + D_N$ in both gas phase and solution. Indeed, with the exception of the $D_N + A_N$ intermediate (which is again destabilised, in this case by 9.1 kcal mol$^{-1}$, by the presence of the solvent) and first transition state (leaving group departure, stabilised by 4.9 kcal mol$^{-1}$), PCM and gas phase relative energies are all within 2.5 kcal mol$^{-1}$ of each other. As with both previous cases, optimisation with a PCM correction results in a change in the PES for the $D_N + A_N$ process and IRC calculations from both transition states lead to asymmetric intermediates similar to those seen for the earlier systems (P–$O_{nuc}$ = 3.43 Å, P–$O_{lg}$ = 2.04 Å and P–$O_{nuc}$ = 2.03 Å, P–$O_{lg}$ = 3.72 Å). Once again, the transition state for the reorganisation step linking these two asymmetric intermediates proved elusive.




**Fig. 7** PES for water attack on $RHPO_4^-$ where R = $CFH_2$. Reactant complex lies towards the upper left corner, product towards the lower right.

Once again, optimisation with the larger augmented TZ basis set produces no discernable difference in stationary point geometries, with only a negligible change in barrier heights (*i.e.*, they are

**Table 4** Energies and key geometric parameters of stationary points for water attack on $RHPO_4^-$ where R = $CFH_2$. Here, RC denotes a reactant complex, TS denotes a transition state, Int. denotes an intermediate, Asym. Int. denotes the asymmetric intermediate found from the IRC with PCM. Parenthesised values indicate PCM optimised results

| | Associative pathway | | | | | Dissociative pathway | | | | | |
|---|---|---|---|---|---|---|---|---|---|---|---|
| | RC | $A_N + D_N$ TS (**1**) | $A_N + D_N$ Int. | $A_N + D_N$ TS (**2**) | PC | RC | $D_N + A_N$ TS (**1**) | $D_N + A_N$ Asym. Int. **1** | $D_N + A_N$ Int. | $D_N + A_N$ Asym. Int. **2** | $D_N + A_N$ TS (**2**) | PC |
| **P–$O_{nuc}$/Å** | 3.36 (3.30) | 2.17 (2.22) | 1.86 (1.78) | 1.68 (1.66) | 1.66 (1.64) | 3.36 (3.30) | 3.11 (3.21) | (3.43) | 3.42 | (2.03) | 1.99 (1.86) | 1.66 (1.64) |
| **P–$O_{lg}$/Å** | 1.69 (1.67) | 1.75 (1.70) | 1.75 (1.78) | 2.33 (2.26) | 3.33 (3.35) | 1.69 (1.67) | 2.06 (1.87) | (2.04) | 3.70 | (3.72) | 3.66 (3.74) | 3.33 (3.35) |
| **Total energy/Hartree** | –858.51978 | –858.46174 | –858.48091 | –858.47492 | –858.52602 | –858.51978 | –858.47513 | (–858.58472) | –858.49773 | (–858.58729) | –858.46892 | –858.52602 |
| **ΔH/kcal mol$^{-1}$** | 0 | 36.4 | 24.4 | 28.2 | –3.9 | 0 | 28.0 | — | 13.8 | — | 31.9 | –3.9 |
| **ΔH (PCM)/kcal mol$^{-1}$** | 0 | 36.8 | 24.8 | 27.6 | –2.8 | 0 | 23.2 | 22.1 | — | 20.4 | 34.4 | –2.8 |




**Fig. 8** Stationary points for $H_2O$ attack on $RHPO_4^-$, where R = $CFH_2$, $A_N + D_N$ pathway. Shown are: (a) the reactant complex; (b) the TS for P–OH formation; (c) the associative intermediate; (d) the TS for P–$OCFH_2$ breaking and (e) the product complex.




**Fig. 9** Stationary points for $H_2O$ attack on $RHPO_4^-$, where R = $CFH_2$, $D_N + A_N$ pathway. Shown are: (a) the reactant complex; (b) the TS for P–$OCFH_2$ breaking; (c) the first asymmetric intermediate; (d) the second asymmetric intermediate; (e) the TS for P–OH formation and (f) the product complex.

raised by 0.6 and 0.8 kcal mol$^{-1}$ for the associative and dissociative pathways, respectively).

Geometries and energies for the system with R = $OCF_2H$ are very similar to R = $OCFH_2$, and are therefore not included in our discussion.

### Phosphate ester hydrolysis, $RHPO_4^-$, R = $CF_3$

Compared to the previous values of ΔPA (up to –30 kcal mol$^{-1}$), that for R = $CF_3$ is quite large at –67.2 kcal mol$^{-1}$, and this is reflected in the potential energy surface (Fig. 10). The associative mechanism for the previous systems followed a stepwise $A_N$ + $D_N$ pathway but when the leaving group is changed to $OCF_3$, the associative mechanism proceeds through a concerted ($A_ND_N$)

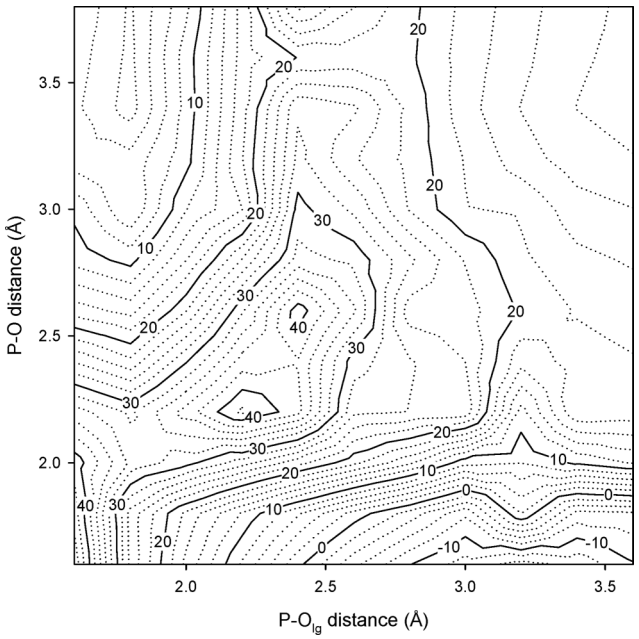


**Fig. 10** PES for water attack on $RHPO_4^-$ where R = $CF_3$. The reactant complex lies towards the upper left corner, product towards lower right.

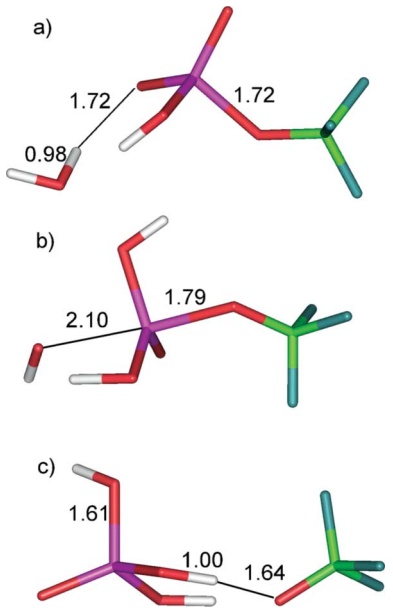


**Fig. 11** Stationary points for $H_2O$ attack on $RHPO_4^-$, where R = $CF_3$, $A_ND_N$ pathway. Shown are: (a) the reactant complex; (b) the $A_ND_N$ TS and (c) the product complex.

pathway. This TS (Fig. 11b) is structurally similar to the first TS in the stepwise $A_N$ + $D_N$ pathways observed with less electron withdrawing leaving groups and the barrier height is similar also, at 36.0 kcal $mol^{-1}$ in the gas phase and 35.9 kcal $mol^{-1}$ when optimised in solution.

The stationary points for the $D_N$ + $A_N$ pathway are shown in Fig. 12 and the key geometric parameters are shown in Table 5. This further increase in leaving group stability results in an increase in P–$O_{lg}$ length in the first transition state, despite stabilising the intermediate. Curiously, proton transfer to the leaving group is observed as the leaving group departs, though this proton must be transferred back on to the phosphate during nucleophilic attack. The PES suggests that the second dissociative TS is found with P–O distances of ~2.5 and 3.25 Å to the nucleophile and leaving group, respectively. However, this is an artefact that arises due to the fact that our two dimensional plot is actually a projection of the full multi-dimensional potential energy surface onto two-dimensions. Unconstrained optimisation on this point yields an actual transition state with P–O distances of 1.84 Å and 3.56 Å to the nucleophile and leaving group, respectively. This system has the lowest barrier to the $D_N$ + $A_N$ pathway apart from R = H (27.7 kcal $mol^{-1}$ in the gas phase and 29.2 kcal $mol^{-1}$ in solution)

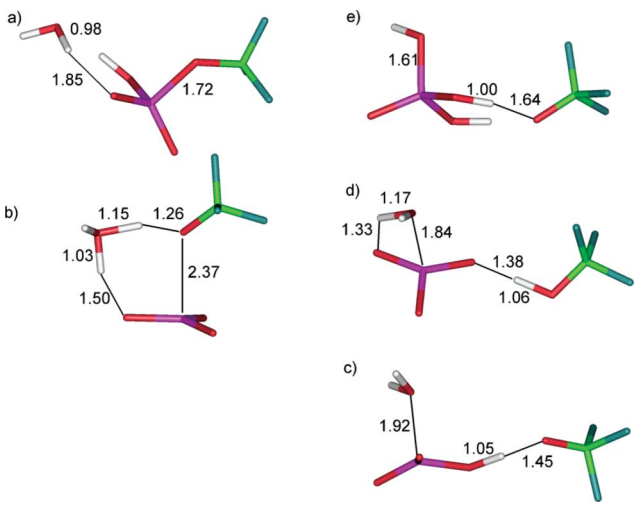


**Fig. 12** Stationary points for $H_2O$ attack on $RHPO_4^-$, where R = $CF_3$, $D_N$ + $A_N$ pathway. Shown are: (a) the reactant complex; (b) the TS for P–$OCF_3$ breaking; (c) the second asymmetric intermediate; (d) the TS for P–OH formation and (e) the product complex.

**Table 5** Energies and key geometric parameters of stationary points for water attack on $RHPO_4^-$ where R = $CF_3$. Here, RC denotes a reactant complex, TS denotes a transition state, Int. denotes an intermediate, Asym. Int. denotes the asymmetric intermediate found from the IRC with PCM. Parenthesised values indicate PCM optimised results

| | Associative pathway | | | Dissociative pathway | | | | | |
|---|---|---|---|---|---|---|---|---|---|
| | RC | $A_ND_N$ TS | PC | RC | $D_N$ + $A_N$ TS (1) | $D_N$ + $A_N$ Int. | $D_N$ + $A_N$ Asym. Int. | $D_N$ + $A_N$ TS (2) | PC |
| **P–$O_{nuc}$/Å** | 3.34 (3.28) | 2.10 (2.10) | 1.63 (1.61) | 3.34 (3.28) | 3.29 (3.34) | 3.42 | (1.92) | 1.96 (1.84) | 1.63 (1.61) |
| **P–$O_{lg}$/Å** | 1.74 (1.72) | 1.83 (1.79) | 3.21 (3.20) | 1.74 (1.72) | 3.10 (2.37) | 3.68 | (3.52) | 3.62 (3.56) | 3.21 (3.20) |
| **Total energy/Hartree** | −1056.99046 | −1056.93303 | −1057.01462 | −1056.99046 | −1056.95516 | −1056.97286 | (−1057.06084) | −1056.94627 | −1057.01462 |
| **ΔH/kcal $mol^{-1}$** | 0 | 36.0 | −15.2 | 0 | 22.2 | 11.0 | — | 27.7 | −15.2 |
| **ΔH (PCM)/kcal $mol^{-1}$** | 0 | 35.9 | −10.5 | 0 | 24.2 | — | 13.5 | 29.2 | −10.5 |

 

**Table 6** Counterpoise energies for an example reaction (first step of the $A_N + D_N$ mechanism for R = $CH_3$) calculated using both 6-31++g(d,p) and augmented cc-pVTZ basis sets. Energies are for gas phase structures and are given in kcal $mol^{-1}$ relative to the reactant complex in all cases. Figures in parentheses indicate the change in relative energy (in kcal $mol^{-1}$) due to the counterpoise correction

| | 6-31++g(d,p) | | | Aug cc-pVTZ | | |
|---|---|---|---|---|---|---|
| | Relative energy | Counterpoise energy (react.-like partitioning) | Counterpoise energy (int.-like partitioning) | Relative energy | Counterpoise energy (react.-like partitioning) | Counterpoise energy (int.-like partitioning) |
| **Reactant** | 0 | 0 | 0 | 0 | 0 | 0 |
| **$A_N + D_N$ TS1** | 38.5 | 39.6 (1.1) | 39.6 (1.1) | 39.6 | 40.5 (0.9) | 40.9 (1.3) |
| **$A_N + D_{N_{int.}}$** | 27.6 | 29.2 (1.6) | 29.3 (1.7) | 29.1 | 30.6 (1.5) | 31.5 (2.4) |

and it is favoured over the $A_ND_N$ pathway by 8.3 kcal $mol^{-1}$ in the gas phase and 6.7 kcal $mol^{-1}$ in solution. For this system, the solvent again modifies the $D_N + A_N$ pathway to include asymmetric intermediates, though only the intermediate with comparatively long $P–O_{lg}$ could be determined. As with all of the previous model systems, optimisation with the larger, triple zeta, basis set results in no detectable change in geometry while barrier heights for both $A_ND_N$ and $D_N + A_N$ processes are increased by less than 1 kcal $mol^{-1}$.

### Basis set superposition error (BSSE)

One potential drawback of the 6-31g and related basis sets is that the double-zeta representation of the valence electrons may result in basis functions being swapped and as a result, complexation energies being overestimated. Though a BSSE can be expected for any atoms that come close together in space, including those bonded to each other, we are only really interested in errors that change as a result of changes in the bonding patterns as the reaction proceeds—it can be argued that the larger BSSEs that result from basis functions being exchanged between bonded atoms are of less interest as they do not change during the reaction as the related bond orders do not change.

While the magnitude of the BSSE can easily be determined using the counterpoise method within Gaussian03, this presents its own problems. As we can see from the results presented here, the partitioning scheme employed within the counterpoise calculation will influence the magnitude of the calculated BSSE. Thus, if we wish to determine the impact of BSSE on reaction barrier heights, it is essential to use the same partitioning scheme throughout the calculations of reaction pathway. Inclusion of all bond making, bond breaking and proton transfer events into a single partitioning scheme results in a total of 5 fragments for inclusion within the counterpoise scheme (see Fig. 13a for details), though two of these fragments consist of individual protons and so have no electrons.

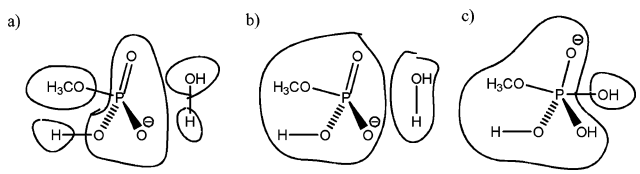


**Fig. 13** Partitioning schemes for use with counterpoise calculations: (a) 5-body partitioning required for consideration of all possible mechanisms using a single consistent partitioning; (b) 2-body partitioning scheme following a reactant-like arrangement, used for the example calculation; (c) 2-body partitioning scheme following an intermediate-like arrangement, also used for the example calculation.

It is not possible to include electron-free fragments within the counterpoise method in Gaussian03 so we need to include these protons in either a reactant-like or product-like partitioning scheme. As these protons are transferred independently, this gives us four permutations of three-body partitioning schemes that would all need to be considered in order to determine full BSSE corrections for each of the reaction schemes described.

Thus we have considered a sample reaction, namely the first step in the $A_N + D_N$ mechanism for R = $CH_3$ to see if the BSSE correction is significant or shows a noticeable difference between the two basis sets considered. This results in two possible two-body partitioning schemes, one reactant-like and one intermediate-like, shown in Fig. 13b and Fig. 13c.

As can be seen from Table 6, application of a counterpoise correction increases the barrier height and destabilises the intermediate for both basis sets to a comparable extent, while the impact of the partitioning scheme is greater for the larger triple-zeta basis set. As the impact of the counterpoise correction is to increase the reaction barrier by approximately 1 kcal $mol^{-1}$ regardless of basis set and partitioning approach, the BSSE is not expected to have any material impact on the conclusions presented here and we do not consider it worthwhile to extend the counterpoise corrections across all reaction pathways or all systems.

## Overview and conclusions

The reaction barriers to both the gas phase and solution reactions (dissociative and the associative mechanisms) for all systems are shown in Table 7, ranked in order of decreasing proton affinity. There is no significant change in barrier height for the associative process despite there being a change in mechanism from $A_N + D_N$ at high proton affinity, to $A_ND_N$ at low PA. Modifying the PA of the leaving group principally affects TS2, corresponding to leaving group departure, which is not generally rate limiting. The most significant change resulting from optimisation within the PCM framework, is in the shape of the overall potential energy surface at long P–O distances. Single point energy calculations showed that the gas phase $D_N + A_N$ intermediate is, in all cases, destabilized when placed within a solvent continuum, whereas reoptimisation in the presence of the continuum suggests in all cases the presence of a rearranged intermediate. IRC calculations from the $D_N + A_N$ transition states reveal a pair of asymmetric intermediates differing in the identity of the oxygen atom forming an electrostatic interaction with the phosphorus.

In contrast to this, the reaction barrier for the $D_N + A_N$ pathway decreases with decreasing PA of the leaving group, with the exception of the water exchange reaction. At first glance, this

**Table 7** A comparison of gas phase and solution reaction barriers for phosphate monoester hydrolysis with various leaving groups. ΔPA denotes the proton affinity difference for each leaving group relative to hydroxide. All values are given in kcal $mol^{-1}$

| | | Associative pathway | | Dissociative pathway | |
|---|---|---|---|---|---|
| Leaving group | ΔPA | Δ*H* | Δ*H* (PCM) | Δ*H* | Δ*H* (PCM) |
| **OH** | 0.00 | 38.5 | 35.8 | 26.9 | 19.8 |
| **$OCH_3$** | −10.8 | 38.7 | 39.2 | 36.5 | 39.0 |
| **$OCFH_2$** | −27.2 | 36.4 | 36.8 | 31.9 | 34.4 |
| **$OCF_3$** | −67.5 | 36.0 | 35.9 | 27.7 | 29.2 |

**Table 8** A comparison of the key geometric parameters for phosphate ester hydrolysis *via* an associative mechanism. It should be noted that the system with the $OCF_3$ leaving group is an anomaly because the reaction actually proceeds *via* an $A_ND_N$ rather than an $A_N + D_N$ mechanism. TS denotes a transition state, and RC and PC denote reactant and product complexes, respectively. All distances are given in Å

| | RC | | $A_N + D_N$ TS1 | | $A_N + D_N$ Intermediate 1 | | $A_N + D_N$ TS2 | | PC | |
|---|---|---|---|---|---|---|---|---|---|---|
| Leaving group | $P–O_{nuc}$ | $P–O_{lg}$ | $P–O_{nuc}$ | $P–O_{lg}$ | $P–O_{nuc}$ | $P–O_{lg}$ | $P–O_{nuc}$ | $P–O_{lg}$ | $P–O_{nuc}$ | $P–O_{lg}$ |
| **OH** | 3.29 | 1.64 | 2.23 | 1.67 | 1.76 | 1.76 | 1.67 | 2.23 | 1.64 | 3.29 |
| **$OCH_3$** | 3.30 | 1.64 | 2.24 | 1.66 | 1.82 | 1.71 | 1.67 | 2.20 | 1.64 | 3.29 |
| **$OCFH_2$** | 3.30 | 1.67 | 2.22 | 1.70 | 1.78 | 1.78 | 1.66 | 2.26 | 1.64 | 3.35 |
| **$OCF_3$** | 3.28 | 1.72 | 2.10 | 1.79 | — | — | — | — | 1.61 | 3.20 |

**Table 9** A comparison of the key geometric parameters for phosphate ester hydrolysis *via* a dissociative mechanism. TS denotes a transition state, and RC and PC denote reactant and product complexes, respectively. All distances are given in Å

| | RC | | $D_N+A_N$ TS1 | | $D_N+A_N$ Intermediate 1 | | $D_N+A_N$ Intermediate 2 | | $D_N+A_N$ TS2 | | PC | |
|---|---|---|---|---|---|---|---|---|---|---|---|---|
| Leaving group | $P–O_{nuc}$ | $P–O_{lg}$ | $P–O_{nuc}$ | $P–O_{lg}$ | $P–O_{nuc}$ | $P–O_{lg}$ | $P–O_{nuc}$ | $P–O_{lg}$ | $P–O_{nuc}$ | $P–O_{lg}$ | $P–O_{nuc}$ | $P–O_{lg}$ |
| **OH** | 3.29 | 1.64 | 3.15 | 1.82 | 3.38 | 1.94 | 1.94 | 3.38 | 1.82 | 3.15 | 1.64 | 3.39 |
| **$OCH_3$** | 3.30 | 1.64 | 3.13 | 1.80 | 3.33 | 1.91 | 2.04 | 3.85 | 1.86 | 3.85 | 1.64 | 3.29 |
| **$OCFH_2$** | 3.30 | 1.67 | 3.21 | 1.87 | 3.43 | 2.04 | 2.03 | 3.72 | 1.86 | 3.74 | 1.64 | 3.35 |
| **$OCF_3$** | 3.28 | 1.72 | 3.34 | 2.37 | — | — | 1.92 | 3.52 | 1.84 | 3.56 | 1.61 | 3.20 |

might be surprising as there is no participation of the leaving group in the rate limiting step, namely attack of the nucleophile. However, decreasing the PA of the leaving group stabilises the whole right-hand edge of our PES, including the TS for attack of the nucleophile (TS2). As this transition state is higher in energy than that for leaving group departure (TS1) in all systems, stabilisation of TS2 results in a lower overall barrier height. In all cases, the nucleophile serves a dual role, also aiding the net transfer of a proton from phosphate to leaving group in the initial bond breaking step whereas only the water exchange reaction shows a similar catalytic role for the leaving group in the second, bond making, step, thus perhaps accounting for its anomalously low reaction barrier. Inclusion of a PCM correction clouds the picture as it serves to stabilise TS1 structures to the extent that in some cases, they are now lower in energy than the PCM-optimised intermediates. Following the IRC and optimising to local minima reveal the presence of asymmetric intermediates from both TS1 and TS2 structures. Presumably these new intermediates are connected by a further transition state, but we have been unable to identify such a structure. It remains questionable whether this modification of the reaction pathway is real or simply an artefact of the cavitation term within the PCM model, as we only see this change at long P–O distances (and therefore large cavities required to accommodate the system). Overall, as the PA of the leaving group decreases, and so stability of the anion increases, the dissociative, $D_N + A_N$, reaction becomes favoured over the associative, $A_N + D_N$, process. For $OCH_3$ as leaving group, there is no clear preference between $A_N + D_N$ and $D_N + A_N$, but for very low PA groups such as $OCF_3$, the $D_N + A_N$ becomes favoured. It is clear, however, that even at very low PA, both associative and dissociative pathways are available and so the balance between them may be affected by external conditions, perhaps to bring the associative mechanism into favour for at least some of the systems presented here.

The key geometric parameters for the associative and dissociative pathways for each system are shown in Tables 8 and 9, respectively. The stationary points along the associative pathways show very little variation with decreasing leaving group proton affinity. In particular, the $A_ND_N$ TS (leaving group = $OCF_3$) corresponds closely to TS1 for the $A_N + D_N$ processes (all other leaving groups). The change in mechanism is solely due to the stabilisation of TS2 (leaving group departure) so that it lies lower in energy than the "intermediate" structure (and is therefore no longer a transition state) for low PA leaving groups. Again, contrasting with this, significant changes are observed in TS1 (leaving group departure) for the dissociative, $D_N + A_N$, process. As the stability of the leaving group increases, so too does the length of $P–O_{lg}$ increase, against expectation from the Hammond postulate. However, in all cases, $P–O_{lg}$ bond cleavage also involves two proton transfers which must be taken into account in any prediction of changes to transition state structure. A lowering of the leaving group PA makes the associated proton transfer less favourable, driving the $P–O_{lg}$ breaking TS towards longer P–O bonds and earlier proton transfer.

 

It has been generally considered that phosphate monoester hydrolysis proceeds *via* a dissociative pathway[2,41,42,44] and some recent computational studies would appear to corroborate this finding.[45] In contrast to this, however, a careful computational study that examined the actual free energy surface for the hydrolysis of the methyl phosphate monoanion[25] showed that both associative and dissociative pathways are equally viable. Similarly, previous studies on phosphate monoester dianions[22] and phosphate diesters[23] have demonstrated that the hydrolysis mechanism is dependent on the acidity of the leaving group, preferring a more compact mechanism at high p$K_a$ and switching to a more expansive mechanism at lower p$K_a$, even for homologous systems. In this work, for the hydrolysis of the methyl phosphate monoanion, we also obtain barriers that are indistinguishable within the error range of the calculations for the associative and dissociative pathways. However, as with previous studies on phosphate monoester dianions and phosphate diesters, we have demonstrated that the nature of the leaving group also affects the potential energy surface of the hydrolysis of phosphate monoester monoanions (for instance in the case of R = $CF_3$, where there is a switch from a stepwise $A_N$ + $D_N$ pathway to a concerted $A_ND_N$ pathway). In the case of the fluorinated leaving groups, we observe a progressive favouring of a dissociative pathway, concomitant with the fact that we have significantly stabilized the leaving group (it is important to note, however, that our study does not take into account the solute configurational entropy, beyond the basic correction in gaussian, which has been demonstrated to be an important factor,[17,23,46] and including this contribution could alter the relative energies of the $A_N$ + $D_N$ and $D_N$ + $A_N$ processes for a given system without altering the overall trends observed here.) It can be argued that our fluorinated leaving groups are not particularly physiological, however, the purpose of this work is to demonstrate that there is a trend even when examining simple systems, free from additional structural complications, and we will be examining more complex systems in a subsequent work. The key point here is that there are multiple factors that affect the preferred choice of mechanism, and that the common assumption that the non-enzymatic hydrolysis of phosphate monoesters proceeds through a dissociative pathway is oversimplified. For example, almost all of the observations used by Westheimer[2] to support a metaphosphate intermediate can also be applied to mechanisms involving a pentavalent intermediate provided one does not make assumptions as to which step is rate determining. Finally, we also demonstrate here the importance of water-mediated proton transfer between the phosphate and leaving group during leaving group departure, though when examining the energetics of this process, it is essential to consider the entropic contribution of this water molecule.

Perhaps the most significant result described here is the involvement of a water molecule in mediating proton transfer between the phosphate and leaving group during leaving group departure. Restricting our systems to include only phosphate, nucleophile and leaving group clearly prevents equivalent interactions during steps involving the nucleophile as the leaving group appears not to fulfil a similar role during nucleophilic attack. It might be tempting therefore to include additional water molecules to mediate further proton transfers but inclusion of additional water molecules in our calculations increases their complexity leading to further problems with configurational entropy. Additionally, as was demonstrated by Kamerlin *et al.*,[46] calculations involving mixed implicit/explicit solvent models are problematic, and the inclusion of extra water molecules is likely to adversely affect the accuracy of our results. Clearly, understanding the factors that control the mechanism of phosphate ester hydrolysis is of absolute importance when attempting to understand the selectivity of the many and varied enzymes that regulate this reaction.

Comparing the results obtained with a 6-31g++(d,p) basis set and a full triple zeta basis set (augmented cc-pVTZ) shows little benefit in terms of calculated reaction barriers or geometries from the larger basis set. Similarly, our test calculation shows little impact of BSSE on the calculated barrier heights and that the impact is similar for both basis sets, though the choice of partitioning scheme can be almost as important as the basis set in determining the magnitude of BSSE correction.

## Acknowledgements

The authors would like to thank the EPSRC for funding (Grant GR/N39968/01), and the University of Birmingham for access to the BlueBear cluster.

## References

1 I. R. Vetter and A. Wittinghofer, *Q. Rev. Biophys.*, 1999, **32**, 1–56.
2 F. H. Westheimer, *Chem. Rev.*, 1981, **81**, 313–326.
3 W. W. Cleland and A. C. Hengge, *Chem. Rev.*, 2006, **106**, 3252–3278.
4 L. Pauling, *J. Am. Chem. Soc.*, 1947, **69**, 542–553.
5 S. C. L. Kamerlin, N. H. Williams and A. Warshel, *J. Org. Chem.*, 2008, **73**, 6960–6969.
6 J. Wilkie and D. Gani, *J. Chem. Soc., Perkin Trans. 2*, 1996, 783–787.
7 S. C. L. Kamerlin and J. Wilkie, *Org. Biomol. Chem.*, 2007, **5**, 2098–2108.
8 D. Easty, W. Gallagher and D. C. Bennet, *Curr. Cancer Drug Targets*, 2006, **6**, 519–532.
9 R. H. van Huijsduijnen, A. Bombrun and D. Swinnen, *Drug Discov. Today*, 2002, **7**, 1013–1019.
10 F. Aguilar-Perez, P. Gomez-Tagle, E. Collado-Fregoso and A. K. Yatsimirsky, *Inorg. Chem.*, 2006, **45**, 9502–9517.
11 M. Padovani, N. H. Williams and P. Wyman, *J. Phys. Org. Chem.*, 2004, **17**, 472–477.
12 T. Humphry, M. Forconi, N. H. Williams and A. C. Hengge, *J. Am. Chem. Soc.*, 2004, **126**, 11864–11869.
13 J. M. Friedman, S. Freeman and J. R. Knowles, *J. Am. Chem. Soc.*, 1988, **110**, 1268–1275.
14 D. Herschlag and W. P. Jencks, *J. Am. Chem. Soc.*, 1989, **111**, 7579–7586.
15 R. H. Hoff and A. C. Hengge, *J. Org. Chem.*, 1998, **63**, 195–195.
16 J. Åqvist, K. Kolmodin, J. Florián and A. Warshel, *Chem. Biol.*, 1999, **6**, R71–R80.
17 S. C. L. Kamerlin, J. Florián and A. Warshel, *ChemPhysChem*, 2008, **9**, 1767–1773.
18 J. M. Mecero, P. Barrett, C. W. Lam, J. E. Fowler, J. M. Ugalde and L. G. Pedersen, *J. Comput. Chem.*, 2000, **21**, 43–51.
19 G. M. Arantes and H. Chaimovich, *J. Phys. Chem. A*, 2005, **109**, 5625–5635.
20 Y. Liu, A. Gregersen, A. Hengge and D. M. York, *Biochemistry*, 2006, **45**, 10043–10053.
21 Y. Liu, B. A. Gregersen, X. Lopez and D. M. York, *J. Phys. Chem. B*, 2006, **109**, 19987–20003.
22 M. Klähn, E. Rosta and A. Warshel, *J. Am. Chem. Soc.*, 2006, **128**, 15310–15323.
23 E. Rosta, S. C. L. Kamerlin and A. Warshel, *Biochemistry*, 2008, **47**, 3725–3735.
24 J. Florián, J. Åqvist and A. Warshel, *J. Am. Chem. Soc.*, 1998, **120**, 11524–11525.
25 J. Florián and A. Warshel, *J. Phys. Chem. B*, 1998, **102**, 719–734.
26 S. C. L. Kamerlin, C. E. McKenna, M. F. Goodman and A. Warshel, *Biochemistry*, 2009, **48**, 5963–5971.

27 M. Dittrich, *Introduction to QM simulations*, Beckman Institute for Advanced Science and Technology, Theoretical and Computational Biocatalysis Group, University of Illinois at Urbana-Champaign, 2003.
28 W. P. Jencks, *Chem. Rev.*, 1985, **85**, 511–527.
29 R. A. More O'Ferrall, *J. Chem. Soc. B*, 1970, 274–277.
30 M. J. Frisch, G. W. Trucks, H. B. Schlegel, G. E. Scuseria, M. A. Robb, J. R. Cheeseman, J. A. Montgomery, Jr., T. Vreven, K. N. Kudin, J. C. Burant, J. M. Millam, S. S. Iyengar, J. Tomasi, V. Barone, B. Mennucci, M. Cossi, G. Scalmani, N. Rega, G. A. Petersson, H. Nakatsuji, M. Hada, M. Ehara, K. Toyota, R. Fukuda, J. Hasegawa, M. Ishida, T. Nakajima, Y. Honda, O. Kitao, H. Nakai, M. Klene, X. Li, J. E. Knox, H. P. Hratchian, J. B. Cross, V. Bakken, C. Adamo, J. Jaramillo, R. Gomperts, R. E. Stratmann, O. Yazyev, A. J. Austin, R. Cammi, C. Pomelli, J. Ochterski, P. Y. Ayala, K. Morokuma, G. A. Voth, P. Salvador, J. J. Dannenberg, V. G. Zakrzewski, S. Dapprich, A. D. Daniels, M. C. Strain, O. Farkas, D. K. Malick, A. D. Rabuck, K. Raghavachari, J. B. Foresman, J. V. Ortiz, Q. Cui, A. G. Baboul, S. Clifford, J. Cioslowski, B. B. Stefanov, G. Liu, A. Liashenko, P. Piskorz, I. Komaromi, R. L. Martin, D. J. Fox, T. Keith, M. A. Al-Laham, C. Y. Peng, A. Nanayakkara, M. Challacombe, P. M. W. Gill, B. G. Johnson, W. Chen, M. W. Wong, C. Gonzalez and J. A. Pople, *GAUSSIAN 03 (Revision E.01)*, Gaussian, Inc., Wallingford, CT, 2004.
31 R. Ditchfield, W. J. Hehre and J. A. Pople, *J. Chem. Phys.*, 1971, **54**, 724–728.
32 R. A. Kendall and T. H. Dunning Jr., *J. Chem. Phys.*, 1992, **96**, 6796–6806.
33 C. Adamo and V. Barone, *J. Chem. Phys.*, 1998, **108**, 664–675.
34 J. Perdew, K. Burke and Y. Wang, *Phys. Rev. B.*, 1996, **54**, 16533–16539.
35 A. D. Becke, *J. Chem. Phys.*, 1993, **98**, 1372–1377.
36 P. J. Stephens, F. J. Devlin, C. F. Chabalowski and M. J. Frisch, *J. Phys. Chem.*, 1994, **98**, 11623–11627.
37 S. C. L. Kamerlin, PhD Thesis, University of Birmingham, 2005.
38 P. Csaszar and P. Pulay, *J. Mol. Struct. (Theochem)*, 1984, **114**, 31–34.
39 J. Tomasi, *Theoretical Chemistry Accounts: Theory Computation and Modeling (Theoretica Chimica Acta)*, 2004, **112**, 184.
40 A. K. Rappé, C. J. Casewit, K. S. Colwell and W. A. Goddard, *J. Am. Chem. Soc.*, 1992, **114**, 10024–10035.
41 S. J. Admiraal and D. Herschlag, *J. Am. Chem. Soc.*, 2000, **122**, 2145–2148.
42 W. W. Butcher and F. Westheimer, *J. Am. Chem. Soc.*, 1955, **77**, 2420–2424.
43 C. A. Bunton, D. R. Llewwellyn, K. G. Oldham and C. A. Vernon, *J. Chem. Soc.*, 1958, 3574–3587.
44 J. B. Vincent, M. W. Crowder and B. A. Averill, *Trends Biochem. Sci.*, 1992, **17**, 105–110.
45 N. Iche-Tarrat, J. C. Barthelat and A. Vigroux, *J. Phys. Chem. B*, 2008, **112**, 3217–3221.
46 S. C. L. Kamerlin, M. Haranczyk and A. Warshel, *ChemPhysChem*, 2009, **10**, 1125–1134.

 